

Boundary-induced phase in epitaxial iron layers

Anna L. Ravensburg¹, Mirosław Werwiński², Justyna Rychły-Gruszecka², Justyn Snarski-Adamski², Anna Elsukova,³
Per O. Å. Persson³, Ján Ruzs¹, Rimantas Brucas⁴, Björgvin Hjörvarsson¹, Peter Svedlindh⁴,
Gunnar K. Pálsson¹ and Vassilios Kapaklis¹

¹Department of Physics and Astronomy, Uppsala University, Box 516, 75120 Uppsala, Sweden

²Institute of Molecular Physics, Polish Academy of Sciences, ul. M. Smoluchowskiego 17, 60-179 Poznań, Poland

³Thin Film Physics Division, Department of Physics, Chemistry and Biology (IFM), Linköping University, 58183 Linköping, Sweden

⁴Department of Materials Science and Engineering, Uppsala University, Box 35, 75103 Uppsala, Sweden



(Received 22 January 2024; revised 15 May 2024; accepted 21 June 2024; published 12 August 2024)

We report on the discovery of a boundary-induced body-centered tetragonal iron phase in thin films deposited on MgAl₂O₄ (001) substrates. We present evidence for this phase using detailed x-ray analysis and *ab initio* density functional theory calculations. A lower magnetic moment and a rotation of the easy magnetization direction are observed, as compared with body-centered cubic iron. Our findings expand the range of known crystal and magnetic phases of iron, providing valuable insights for the development of heterostructure devices using ultrathin iron layers.

DOI: [10.1103/PhysRevMaterials.8.L081401](https://doi.org/10.1103/PhysRevMaterials.8.L081401)

The magnetic properties of iron are multifaceted. This is reflected in the results obtained from investigations on the electric control of magnetic domains [1], magnetic anisotropy [2–4], magnetic damping [5], as well as magnetic interface effects [6–8]. Not only are single layers of Fe of relevance, but also Fe in multilayers and superlattices such as Fe/Cr [9,10], Fe/V [11], Fe/Au [12], Fe/MgO [13–15], or Fe/MgAl₂O₄ [16–20] exhibits nontrivial properties. The epitaxial matching of the layers is of particular importance [21,22] since strain and crystal structure can have large effects on the magnetic properties [23–26]. For example, iron can be ferromagnetic, low-spin or high-spin, antiferromagnetic, or even nonmagnetic [23–25], all depending on its tetragonal distortion (c/a) and unit cell volume. Therefore, access to unstrained ultrathin Fe layers is of large importance to enable the separation of boundary and strain effects.

Recently, it was found that Fe (001) layers can be epitaxially grown on single-crystalline MgAl₂O₄ (001) substrates [5,27,28]. A 45° in-plane rotation of the Fe unit cell relative to the unit cell of the substrate, provides growth conditions with an epitaxial misfit of only –0.2% compared with bulk body-centered cubic (bcc) Fe (001) [16,28–30]. Thus, the tetragonal distortion is expected to be low, and the Fe film is structurally similar to bcc Fe. Consequently, the crystal quality of Fe (001) layers can be significantly improved, as compared with Fe layers grown on MgO (001) [5,28,31] or Al₂O₃ (11 $\bar{2}$ 0) [32]. This opens up new alternatives to investigate the effects of layer thickness on, e.g., the magnetic properties of Fe, with

only minor substrate-induced strain effects, which is explored in this letter.

The Fe films were deposited using direct current magnetron sputtering, with nominal thicknesses t_{Fe} in the range of 6–100 Å, at a substrate temperature of 619(2) K. All films were capped at ambient temperature with Pd, Pt, or Al₂O₃. The purpose of the capping is to protect the Fe layer from oxidation. Measuring identical Fe layers with different capping layers allowed us to explore the effect of the outer boundary on the investigated properties. Representative x-ray diffraction patterns using Cu $K_{\alpha 1}$ radiation around the specular Fe (002) Bragg peak of three samples with 25, 50, and 100 Å Fe layer thicknesses are displayed in Fig. 1. As seen in the figure, the peak intensity, position, and shape are different for these samples. The intensity is found to increase quadratically with increasing thickness, as expected for fully structurally coherent layers [33,34]. Furthermore, the positions of the Fe (002) Bragg peak are shifted toward smaller angles with decreasing thickness of the layers. The out-of-plane atomic distance d in Fe layers of 25, 50, and 100 Å thicknesses is elongated compared with equilibrium bcc Fe [35,36], with the average out-of-plane lattice parameters c_0 along [001] being 2.9088(8), 2.8856(1), and 2.8738(2) Å, respectively. Hence, the average out-of-plane lattice parameter is consistent with a tetragonal distortion, which appears to increase with decreasing film thickness [16,28–30]. The full width at half maximum (FWHM) of the Fe (002) rocking curves are all <0.04°, independent of layer thickness, consistent with near-perfect single crystalline growth of all these layers. An atomic registry of the interface between Fe and the substrate was confirmed with atomic-resolved high-angular annular dark-field scanning transmission electron microscopy imaging. Furthermore, no evidence for any oxidation or structural damage was found near the interface (see the Supplemental Material (SM) [37]).

The observation of Laue oscillations around the Fe (002) Bragg peak (see Fig. 1) for all three samples [28,38,39]

Published by the American Physical Society under the terms of the Creative Commons Attribution 4.0 International license. Further distribution of this work must maintain attribution to the author(s) and the published article's title, journal citation, and DOI. Funded by Bibsam.

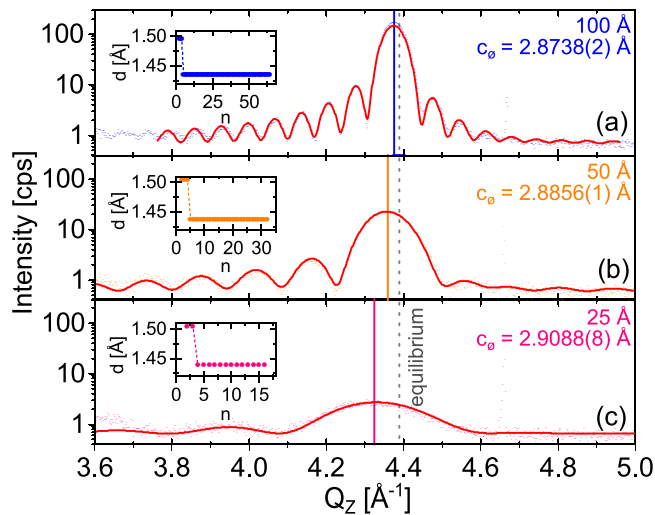


FIG. 1. X-ray diffraction patterns around the Fe (002) Bragg peak of (a) 100-Å-thick, (b) 50-Å-thick, and (c) 25-Å-thick Fe films grown on MgAl_2O_4 (001). Fits are shown as red lines. The corresponding out-of-plane lattice parameter c_ϕ is shown on the right. Insets: Evolution of the out-of-plane atomic distance d as a function of the number of atomic monolayers n .

provides additional information on the structural coherency. The asymmetry in the intensity of the Laue oscillations around the (002) peak is consistent with the presence of a change in out-of-plane interplanar atomic spacing in the Fe layers [39–42]. To obtain information on the shape of the profile of the interplanar spacing, we performed simulations of the Bragg peak and the Laue oscillations (see the SM [37]) using GENL [39]. The results of the fitting illustrated in Fig. 1 are consistent with the presence of two distinct coherently scattering regions in all samples: 3–4 monolayers (ML) closest to the substrate with large tetragonal out-of-plane distortion ($d = 1.50 \text{ \AA}$), while the rest of the films have a lattice parameter close to unstrained Fe.

In Fig. 2(a) we illustrate a summary of the results from the structural analysis, including asymmetric reflections, namely, the Fe (002) and (112) Bragg peaks (see the SM [37] for details and Refs. [45–48] therein). As seen in the figure, the average out-of-plane lattice parameter c_ϕ scales with the inverse thickness of the layers. The results were fitted using

$$c_\phi = c_1 \left(1 - \frac{t_\Delta}{t_{\text{Fe}}} \right) + c_2 \frac{t_\Delta}{t_{\text{Fe}}}, \quad (1)$$

where c_1 and c_2 denote the out-of-plane lattice parameters of the two regions, and t_Δ denotes the extension of the region closest to the substrate. The intercept of the y axis corresponds to infinitely thick Fe layers, with negligible contribution from the interface region. From the fitting, we get $c_1 = 2.862(5) \text{ \AA}$, which is within the uncertainty identical to the unstrained lattice parameter of bcc Fe (2.866 \AA) [35]. The slope of the fit in Fig. 2(a) is proportional to the thickness of the interface layers t_Δ and the difference in the lattice parameters of the two regions ($c_2 - c_1$) $t_\Delta = 0.58(5) \text{ \AA}^2$. The corresponding values of $(c_2 - c_1)t_\Delta$ from the fitting of the diffraction data (see Fig. 1) are 0.56 , 0.79 , and 0.56 \AA^2 for the 100-, 50-, and 25-Å-thick layers, respectively. The extension of the interface

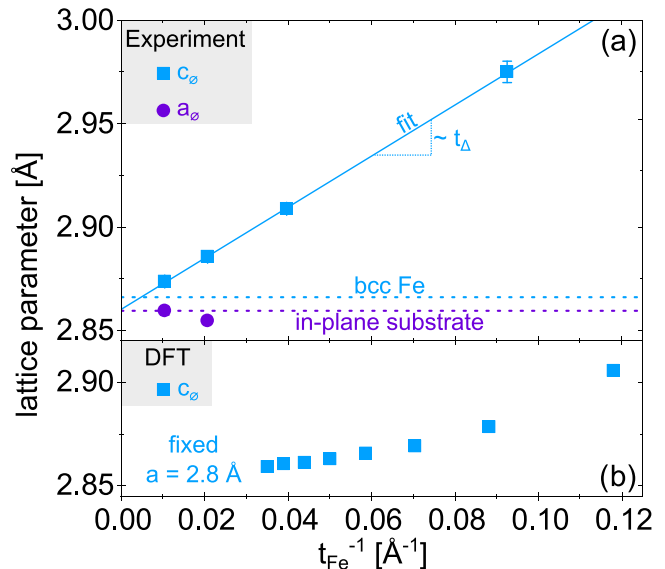


FIG. 2. (a) Experimental in-plane a_ϕ and out-of-plane c_ϕ lattice parameters for epitaxial Fe films with different layer thicknesses t_{Fe} . The Fe layers are capped with Pd. The choice of capping material did not affect the results, see the SM [37] (and Refs. [43,44] therein) for details. The dashed lines correspond to the equilibrium values of bcc Fe [35,36] and the MgAl_2O_4 substrate, while the solid line shows the fit of Eq. (1) to the data. (b) DFT calculated average out-of-plane lattice parameter c_ϕ for a fixed in-plane lattice parameters $a = 2.8 \text{ \AA}$ plotted over inverse Fe layer thickness t_{Fe}^{-1} .

layer needs to be $< 11 \text{ \AA}$, as the data point from that sample is captured by the model in Fig. 2. Thus, the analysis of the diffraction data and the modeling of the shift of the (002) peak are consistent.

For the samples with 100- and 50-Å-thick Fe layers, the average in-plane lattice parameter a_ϕ was determined to be $2.860(2)$ and $2.856(3) \text{ \AA}$, respectively, which closely matches the substrate (2.859 \AA) [49]. Consequently, if the tetragonal distortion of the interface region originated from an elastic response to the biaxial strain, this would correspond to 0.91 in Poisson's ratio equivalent, i.e., the ratio of transverse to longitudinal extension strain, which is not physical for isotropic materials [50,51]. Hence, the tetragonal unit cell distortion is not strain induced, in contrast with other observed nonequilibrium Fe crystal structures like, e.g., body-centered tetragonal (bct) Fe on Ir (001) [52,53] or face-centered cubic (fcc) Fe on Ir (111) [52] or fcc Fe on Cu (001) [54], which are reported to be stabilized through epitaxy.

We used density functional theory (DFT) calculations to explore the contribution of finite-sized effects on the obtained results. Consequently, first, the calculations were performed on freestanding Fe layers. The total energy for a tetragonally distorted bct structure was found to be lower than that obtained for bcc when the thickness was < 9 ML (see the SM [37] and Refs. [55–58] therein). For biaxially clamped Fe layers with $c/a > 1$, corresponding to the same strain state as experimentally determined for Fe on MgAl_2O_4 (001), the calculated average out-of-plane lattice parameter c_ϕ is plotted as a function of inverse Fe layer thickness in Fig. 2(b). A profound tetragonal distortion is obtained for layers in the

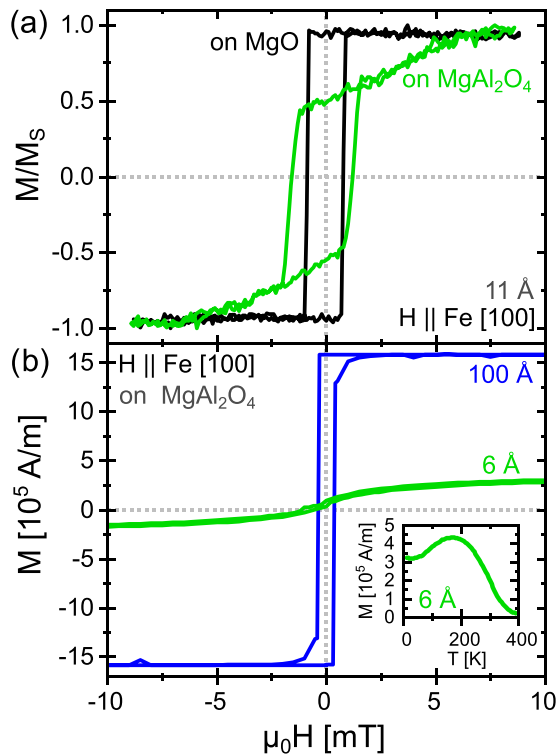


FIG. 3. Easy axis magnetic hysteresis of (a) thin films of 11 Å Fe grown on MgAl_2O_4 (001) and MgO (001), capped with 50 Å Pd and measured using a longitudinal magneto-optical Kerr effect (L-MOKE) setup and (b) 6 and 100 Å Fe grown on MgAl_2O_4 (001) capped with 50 Å Al_2O_3 measured in a superconducting quantum interference device (SQUID). The measurements were conducted at ambient temperature. Inset: Magnetization of the 6 Å Fe layer at a constant applied field of 5 mT as a function of temperature.

few-ML limit, while the obtained effect is thickness dependent. The effect decreases with increasing film thickness, giving rise to a change in slope, as seen in Fig. 2(b). Considering the size of the calculated effect and the observed changes with thickness, we conclude that the contribution from finite size to the experimentally found structural distortion is small, as compared with the interface effect described above.

Having established the presence of an interface layer with a deviating lattice parameter, we now turn our attention to its effects on the magnetic properties. Hysteresis curves that were measured with an applied field along the bulk Fe in-plane magnetic easy axis direction, i.e., Fe [100] of 11 Å Fe layers deposited simultaneously on MgAl_2O_4 (001) and MgO (001), are shown in Fig. 3(a). A square-shaped hysteresis curve is observed for the Fe layer on MgO (001), typical for an easy axis magnetization loop, in stark contrast with the Fe layer deposited on MgAl_2O_4 (001). Measurements with applied field along the bulk Fe in-plane magnetic hard axis direction, i.e., Fe [110], confirm a hard axis behavior for the sample on MgO and an increased remanence for the sample on MgAl_2O_4 (see the SM [37] for details and Ref. [59] therein). These observations are consistent with an exchange of easy and hard axes when Fe is grown on MgAl_2O_4 (001) and MgO (001) substrates, respectively. Measurements of the out-of-plane component of the magnetization do not indicate

an out-of-plane contribution to the magnetization, which can, however, not be excluded as an explanation for the moment reduction. The main effect is attributed to the electronic effects at the boundary in combination with some contribution from the finite size of the layers, which is in line with the sole observation of a reduced magnetic moment for the thinnest, i.e., 6-Å-thick Fe layer.

The contribution of the interface region to the overall magnetic properties can also be inferred by comparing samples with vastly different thicknesses. For instance, Fig. 3(b) displays hysteresis curves measured along the Fe [100] direction for 6 and 100 Å Fe layers deposited on MgAl_2O_4 (001). The absolute magnetization of the sample with 100 Å Fe layer thickness is $M_S = 1.588 \times 10^6$ A/m; $\mu_0 M_S = 1.99$ T, which is slightly smaller than for bulk Fe, where $\mu_0 M_S = 2.15$ T [60]. The difference is attributed to the finite layer thickness. For the thinner 6 Å Fe layer, we observe a reduction in the saturation magnetization, accompanied also by a distinct change in the shape of the hysteresis curve. The temperature-dependent magnetization of the 6 Å Fe layer was determined in an applied magnetic field of 5 mT along the Fe [100] direction. An initial increase with decreasing temperature is observed, followed by a decrease with decreasing temperature <150 K. These observations are consistent with an increase in magnetic anisotropy, exceeding the torque provided by the external field at ~ 150 K, in line with the conclusions above. The tetragonal distortion at the interface is not the only factor affecting the magnetic properties. For example, Fe forms Fe-O bonds at the MgAl_2O_4 (001) interface [16,31], which can contribute to lower magnetization, a change in the magnetic anisotropy, as well as lower Curie temperature. For the 6 Å Fe layer, the contribution of finite-sized effects on the ordering temperature is nonnegligible and can be determined by empirical models, as seen in Zhang and Willis [61] and Xin *et al.* [62].

In summary, we have identified a boundary-induced state in Fe at the interface with a MgAl_2O_4 (001) substrate. The interface state in Fe is argued to result from an electronic proximity effect with the substrate. The easy axis of the observed bct phase is rotated by $\pi/4$ as compared with bulk Fe, which gives rise to changes in the obtained anisotropy with thickness. These findings add to the understanding and optimal design of ML-thick Fe layers in heterostructures such as Fe/ MgO or Fe/ MgAl_2O_4 , which hold a potential for magnetic tunnel junctions and future three-dimensional memory storage devices.

The data that support the findings of this paper are available from the authors upon reasonable request.

V.K. and P.S. acknowledge financial support from the Swedish Research Council (Projects No. 2019-03581 and No. 2021-04658). G.K.P. acknowledges funding from the Swedish Energy Agency (Project No. 2020-005212). M.W., J.R.G., and J.S.A. acknowledge financial support from the National Science Center Poland under Decisions No. DEC-2018/30/E/ST3/00267 (SONATA-BIS 8) and No. DEC-2019/35/O/ST5/02980 (PRELUDIUM-BIS 1). The authors also acknowledge access to the Swedish National Infrastructure for Advanced Electron Microscopy, ARTEMI, supported

by the Swedish Research Council (VR) and the Foundation for Strategic Research (SSF), through Grants No. 2021-00171 and No. RIF21-0026. J.R. acknowledges financial support from the Swedish Research Council (Grant No. 2021-03848),

Olle Engkvist's Foundation (Grant No. 214-0331) and Knut and Alice Wallenberg Foundation (Grant No. 2022.0079). The authors would like to thank Christina Vantaraki for AFM measurements.

- [1] P. Gospodarič, E. Młyńczak, I. Soldatov, A. Kákay, D. E. Bürgler, L. Plucinski, R. Schäfer, J. Fassbender, and C. M. Schneider, *Phys. Rev. Res.* **3**, 023089 (2021).
- [2] H. J. Elmers and U. Gradmann, *Appl. Phys. A* **51**, 255 (1990).
- [3] R. Allenspach and A. Bischof, *Phys. Rev. Lett.* **69**, 3385 (1992).
- [4] N. Metoki, M. Hofelich, T. Zeidler, T. Mühge, C. Morawe, and H. Zabel, *J. Magn. Magn. Mater.* **121**, 137 (1993).
- [5] B. Khodadadi, A. Rai, A. Sapkota, A. Srivastava, B. Nepal, Y. Lim, D. A. Smith, C. Mewes, S. Budhathoki, A. J. Hauser, M. Gao, J.-F. Li, D. D. Viehland, Z. Jiang, J. J. Heremans, P. V. Balachandran, T. Mewes, and S. Emori, *Phys. Rev. Lett.* **124**, 157201 (2020).
- [6] T. Urano and T. Kanaji, *J. Phys. Soc. Jpn.* **57**, 3403 (1988).
- [7] J. Balogh, I. Dézsi, C. Fetzter, J. Korecki, A. Kozioł-Rachwał, E. Młyńczak, and A. Nakanishi, *Phys. Rev. B* **87**, 174415 (2013).
- [8] F. Ibrahim, A. Hallal, A. Kalitsov, D. Stewart, B. Dieny, and M. Chshiev, *Phys. Rev. Appl.* **17**, 054041 (2022).
- [9] P. Etienne, G. Creuzet, A. Friederich, F. Nguyen-Van-Dau, A. Fert, and J. Massies, *Appl. Phys. Lett.* **53**, 162 (1988).
- [10] S. S. P. Parkin, N. More, and K. P. Roche, *Phys. Rev. Lett.* **64**, 2304 (1990).
- [11] B. Hjörvarsson, J. A. Dura, P. Isberg, T. Watanabe, T. J. Udovic, G. Andersson, and C. F. Majkrzak, *Phys. Rev. Lett.* **79**, 901 (1997).
- [12] A. Fuß, S. Demokritov, P. Grünberg, and W. Zinn, *J. Magn. Magn. Mater.* **103**, L221 (1992).
- [13] J. Faure-Vincent, C. Tiusan, C. Bellouard, E. Popova, M. Hehn, F. Montaigne, and A. Schuhl, *Phys. Rev. Lett.* **89**, 107206 (2002).
- [14] R. Moubah, F. Magnus, T. Warnatz, G. K. Pálsson, V. Kapaklis, V. Ukleev, A. Devishvili, J. Palisaitis, P. O. A. Persson, and B. Hjörvarsson, *Phys. Rev. Appl.* **5**, 044011 (2016).
- [15] F. Magnus, T. Warnatz, G. K. Pálsson, A. Devishvili, V. Ukleev, J. Palisaitis, P. O. A. Persson, and B. Hjörvarsson, *Phys. Rev. B* **97**, 174424 (2018).
- [16] H. Sukegawa, H. Xiu, T. Ohkubo, T. Furubayashi, T. Niizeki, W. Wang, S. Kasai, S. Mitani, K. Inomata, and K. Hono, *Appl. Phys. Lett.* **96**, 212505 (2010).
- [17] Y. Miura, S. Muramoto, K. Abe, and M. Shirai, *Phys. Rev. B* **86**, 024426 (2012).
- [18] M. Belmoubarik, H. Sukegawa, T. Ohkubo, S. Mitani, and K. Hono, *Appl. Phys. Lett.* **108**, 132404 (2016).
- [19] K. Masuda and Y. Miura, *Phys. Rev. B* **96**, 054428 (2017).
- [20] Q. Xiang, R. Mandal, H. Sukegawa, Y. K. Takahashi, and S. Mitani, *Appl. Phys. Express* **11**, 063008 (2018).
- [21] V. Martin, W. Meyer, C. Giovanardi, L. Hammer, K. Heinz, Z. Tian, D. Sander, and J. Kirschner, *Phys. Rev. B* **76**, 205418 (2007).
- [22] D. Sander, *Rep. Prog. Phys.* **62**, 809 (1999).
- [23] V. L. Moruzzi, P. M. Marcus, and J. Kübler, *Phys. Rev. B* **39**, 6957 (1989).
- [24] S. Andrieu, F. L. Razafindramisa, E. Snoeck, H. Renevier, A. Barbara, J. M. Tonnerre, M. Brunel, and M. Piecuch, *Phys. Rev. B* **52**, 9938 (1995).
- [25] M. Friák, M. Šob, and V. Vitek, *Phys. Rev. B* **63**, 052405 (2001).
- [26] T. Burkert, L. Nordström, O. Eriksson, and O. Heinonen, *Phys. Rev. Lett.* **93**, 027203 (2004).
- [27] A. J. Lee, J. T. Brangham, Y. Cheng, S. P. White, W. T. Ruane, B. D. Esser, D. W. McComb, P. C. Hammel, and F. Yang, *Nat. Commun.* **8**, 234 (2017).
- [28] A. L. Ravensburg, G. K. Pálsson, M. Pohlit, B. Hjörvarsson, and V. Kapaklis, *Thin Solid Films* **761**, 139494 (2022).
- [29] S. M. Hosseini, *Phys. Status Solidi (b)* **245**, 2800 (2008).
- [30] I. Ganesh, *Int. Mater. Rev.* **58**, 63 (2013).
- [31] H. L. Meyerheim, R. Popescu, J. Kirschner, N. Jedrecy, M. Sauvage-Simkin, B. Heinrich, and R. Pinchaux, *Phys. Rev. Lett.* **87**, 076102 (2001).
- [32] T. Möhge, A. Stierle, N. Metoki, H. Zabel, and U. Pietsch, *Appl. Phys. A* **59**, 659 (1994).
- [33] P. F. Fewster, *Rep. Prog. Phys.* **59**, 1339 (1996).
- [34] M. Birkholz, in *Thin Film Analysis by X-Ray Scattering* (John Wiley and Sons, Ltd, Weinheim, 2005), Chap. 1, pp. 1–40.
- [35] J. L. Vassent, M. Dynna, A. Marty, B. Gilles, and G. Patrat, *J. Appl. Phys.* **80**, 5727 (1996).
- [36] G. Chiarotti, *Interaction of Charged Particles and Atoms with Surfaces* (Springer, Berlin, 1995).
- [37] See Supplemental Material at <http://link.aps.org/supplemental/10.1103/PhysRevMaterials.8.L081401> for the detailed description of the methods for data analysis and supporting experimental findings.
- [38] A. J. Ying, C. E. Murray, and I. C. Noyan, *J. Appl. Cryst.* **42**, 401 (2009).
- [39] A. L. Ravensburg, J. Bylin, G. K. Pálsson, and V. Kapaklis, [arXiv:2310.13539](https://arxiv.org/abs/2310.13539).
- [40] I. Vartanyants, C. Ern, W. Donner, H. Dosch, and W. Caliebe, *Appl. Phys. Lett.* **77**, 3929 (2000).
- [41] I. Robinson and I. Vartanyants, *Appl. Surf. Sci.* **182**, 186 (2001).
- [42] A. M. Miller, M. Lemon, M. A. Choffel, S. R. Rich, F. Harvel, and D. C. Johnson, *Z. Naturforsch. B* **77**, 313 (2022).
- [43] C. T. Campbell, *Surf. Sci. Rep.* **27**, 1 (1997).
- [44] T. P. A. Hase, M. S. Brewer, U. B. Arnalds, M. Ahlberg, V. Kapaklis, M. Björck, L. Bouchenoire, P. Thompson, D. Haskel, Y. Choi, J. Lang, C. Sánchez-Hanke, and B. Hjörvarsson, *Phys. Rev. B* **90**, 104403 (2014).
- [45] M. Björck and G. Andersson, *J. Appl. Cryst.* **40**, 1174 (2007).
- [46] A. Glavic and M. Björck, *J. Appl. Cryst.* **55**, 1063 (2022).
- [47] J. Birch, J. Sundgren, and P. F. Fewster, *J. Appl. Phys.* **78**, 6562 (1995).
- [48] J. Schroeder, A. Ingason, J. Rosén, and J. Birch, *J. Cryst. Growth* **420**, 22 (2015).
- [49] P. Villars, K. Cenzual, J. Daams, R. Gladyshevskii, O. Shcherban, V. Dubenskyy, N. Melnichenko-Koblyuk, O. Pavlyuk, S. Stoiko, and L. Sysa, *Structure Types. Part 1: Space Groups (230)Ia-3d-(219)-F43-c MgAl₂O₄: Datasheet from Landolt-Börnstein—Group III Condensed Matter Volume 43A1* (Springer, Berlin, 2004).
- [50] K. W. Wojciechowski, *J. Phys. Soc. Jpn.* **72**, 1819 (2003).

- [51] C. W. Huang, W. Ren, V. C. Nguyen, Z. Chen, J. Wang, T. Sritharan, and L. Chen, *Adv. Mater.* **24**, 4170 (2012).
- [52] M. Piecuch, S. Andrieu, J. F. Bobo, and P. Bauer, *Magnetism and Structure in Systems of Reduced Dimension*, edited by R. F. C. Farrow, B. Dieny, M. Donath, A. Fert, and B. D. Hermsmeier (Springer, New York, 1993).
- [53] S. Andrieu, M. Piecuch, H. Fischer, J. Bobo, F. Bertran, P. Bauer, and M. Hennion, *J. Magn. Magn. Mater.* **121**, 30 (1993).
- [54] S. Müller, P. Bayer, C. Reischl, K. Heinz, B. Feldmann, H. Zillgen, and M. Wuttig, *Phys. Rev. Lett.* **74**, 765 (1995).
- [55] M. Methfessel and A. T. Paxton, *Phys. Rev. B* **40**, 3616 (1989).
- [56] P. E. Blöchl, O. Jepsen, and O. K. Andersen, *Phys. Rev. B* **49**, 16223 (1994).
- [57] K. Koepnick and H. Eschrig, *Phys. Rev. B* **59**, 1743 (1999).
- [58] J. P. Perdew, K. Burke, and M. Ernzerhof, *Phys. Rev. Lett.* **77**, 3865 (1996).
- [59] Y. Park, E. E. Fullerton, and S. D. Bader, *Appl. Phys. Lett.* **66**, 2140 (1995).
- [60] J. Solano, O. Gladii, P. Kuntz, Y. Henry, D. Halley, and M. Bailleul, *Phys. Rev. Mater.* **6**, 124409 (2022).
- [61] R. Zhang and R. F. Willis, *Phys. Rev. Lett.* **86**, 2665 (2001).
- [62] X. Xin, G. K. Pálsson, M. Wolff, and B. Hjörvarsson, *Phys. Rev. Lett.* **113**, 046103 (2014).